Effects of Suction-Type Active Flow Control on Wind Turbine Noise and Aerodynamic Performance

Hugo Loureiro da Silva
hugo.da.silva@tecnico.ulisboa.pt

Instituto Superior Técnico, Lisboa, Portugal

July 2016

Abstract

The first objective of the work was to develop an automated meshing script, capable of creating structured C-type meshes around an airfoil with refinement on user-defined number, position and division of suction patches, on the suction side. The mesh file would be used with the DLR developed RANS solver *FLOWer*to perform computations, and the results should be post-processed to be compatible with the IAG developed acoustic code *Rnoise*, to calculate trailing edge noise.

A NACA 64-618 airfoil, with a chord length of 2.5175 m, with Angle of Attack (AOA) of 7.3 $^\circ$, Reynolds number of 11049876 and Mach number (MN) of 0.19, was analysed. The suction patch started at 57.5% of the chord and ended at 62.5%. The suction coefficient c_q was varied between 0 and -0.016, in 6 discrete values. Noise reductions up to 5.2 dB were calculated with the maximum considered suction. However, high suction levels decrease performance in the c_l/c_d ratio, halving it. Lower suction levels (c_q=-0.001) increase performance 10% and accounts for 33% of the total noise reduction observed.

Similar studies were done whilst varying patch configurations, MN and AOA. Results revealed that longer, upstream patches provide a better balance of noise reduction and performance increase at lower suction levels. Higher AOA cases benefited more from the effects of suction, nullifying their baseline increased noise and drag compared to lower AOA cases. Higher MN cases benefited more from noise reduction, but the overall noise emitted was still higher than their lower MN counterparts.
Keywords: Active Flow Control; Trailing Edge Noise; Suction Patch; Performance; Turbulence

1. Introduction

There is, in (almost) every one of us, an innate desire to make the World a better place, be it for selfless and/or selfish reasons. As an engineer, one tends to contribute to that cause by understanding the inner workings of the Universe - the so called Laws of Physics - and finding a way to apply them so that the outcome pushes Humanity a step forward, in one way or another.

With the increase in population numbers comes a necessity to expand residential areas and provide more power for daily activities. Due to global policies to preserve the environment and revert climate change, renewable energy sources are becoming a larger target of investment, and becoming more present in the daily lives of people around the world. As a consequence, at the same time that residential areas grow, so do areas dedicated for renewable energy generation, like solar farms and wind farms. It is a fact that wind turbines create discontent in the population living near to them, due to their noise [1]. Despite there being no proven diseases caused by it [2], sleep disturbances have been associated with the noise [3]. The increasing proximity between residential areas and wind turbines make annoyance complaints due to wind turbines more prevalent, and this technology will gain a bad image before the population, and the investment flowing into it will plummet.

Therefore it is the job of researchers and engineers to solve the noise problem so that turbines and people can coexist without lowering the quality of life. To that effect, Oerlemans *et al.* have investigated the sources of noise in wind turbines and have discovered that most of the noise emitted comes from the trailing edge of the outer regions of the blade, and it was found to scale with $U^{4.5}/U^5$ [4, 5]. This is called turbulent trailing edge noise (TEN).

Wagner explains that turbulence is actually a bad radiator of sound, due to its *quadrupole* nature. However, when the turbulent eddies interact with the sharp trailing edge, the scattering that occurs changes the quadrupole radiation into dipole radiation, which is much more efficient at radiating sound [6]. It was also discovered that the pa-

rameters that influenced noise were the eddy convection velocity (U), the angle which the convecting stream makes with the edge ($\bar{\theta}$), the turbulent length scales (l) and the normalized turbulence intensity (α), which is related to the turbulent kinetic energy [7, 8]. This is visible in (1) :

$$I \propto \rho_0 c_0^3 \cos^3(\bar{\theta}) M^5 \frac{sl}{r^2} \alpha^2, \tag{1}$$

where c_0 is the speed of sound, ρ is the air density, r is the distance and M the Mach number.

Knowing this, researchers have been trying to optimize airfoil geometry to reduce these parameters, and thus reducing noise, with success [9, 10, 11]. But first, better noise prediction models had to be developed, and many are based on the TNO model [12]. Research on this topic allowed for the development of the acoustic code used in this work, *Rnoise*[13], which makes use of the TNO model to find the spectrum of the pressure fluctuations, and afterwards calculate the noise emitted by the trailing edge, by representing the surface pressure fluctuations as a distribution of harmonic evanescent waves and solving the diffraction problem according to [14]:

$$G_{ff}(\omega) = \frac{1}{2\pi R^2} \frac{\omega \acute{L}}{c_0} \int_0^\infty \frac{P(k_1, 0, \omega)}{|k_1|} dk_1, \omega \in [0, \infty]. \tag{2}$$

Finally, by substituting the TNO model pressure fluctuations equation in (2), the total far-field noise spectra level in terms of Sound Pressure Level (SPL) in dB can be computed:

$$L_p(f) = 10 \cdot log \left[\frac{2\pi \cdot G_{ff}(\omega) \cdot df}{4 \cdot 10^{-10}} \right]. \tag{3}$$

Another research direction focused on the development of passive flow control methods, such as serrated and slotted trailing edges, to reduce TEN. Howe's predicted 20 dB results [15] with these methods were never achieved in experiments, likely due to three-dimensional flow effects, but the reductions are nevertheless substantial [16, 17, 10].

On another interesting field that joins aerodynamics and control, Active Flow Control (AFC), researchers have developed actuators of various kinds that can control the flow parameters, thus increasing airfoil performance. Zero-net-mass-flux actuators, plasma actuators, and suction actuators can effectively control the boundary layer parameters and provide increases in lift and critical angle of attack, and decreases in drag [18, 19, 20, 21].

Combining the knowledge of both fields, researchers at the Institut für Aerodynamik und Gasdynamik (IAG) of the University of Stuttgart, have been experimenting with ways to use AFC for TEN reduction. By studying the way that the boundary layer should be influenced by an actuator to reduce noise, it was concluded that suction type actuators could be an answer to the TEN problem, since they effectively reduce boundary layer thickness and turbulent kinetic energy – two factors responsible for TEN [22]. Further research on suction enabled the measurement in a wind tunnel of an SPL reduction of 6 dB, for a static blade portion with suction actuators [23], thus legitimizing suction as a viable means to reduce noise. Numerical investigations on suction have underpredicted this value, however [24, 25]. This work is contribution towards this ongoing research topic.

In regards to the suction actuators themselves, these work by having a perforated part of the airfoil's surface, leading to a suction chamber where pressure is lowered via the use of suction pumps. The lower pressure in the chamber relative to the flow running along the airfoil results in it being sucked. The coefficient of suction, c_q is given by:

$$c_q = \frac{\dot{m}_s}{\rho_\infty \cdot U_\infty \cdot A_s}, \tag{4}$$

where $\dot{m}_s$ represents the mass flow rate, A_s the suction area, ρ_∞ the air density and U_∞ the inflow velocity. Negative values of c_q indicate suction. From the mass flow coefficient it is also possible to calculate the suction speed, as in equation (5):

$$\mid V_s \mid = \frac{\mid c_q \mid U_\infty}{l_{afc}}, \tag{5}$$

where V_s is the suction speed, and l_{afc} is the non-dimensional fraction of the chord which undergoes suction, given by $l_{afc} = l_a/c$, where l_a is the length of the suction actuator, and *c* is the total chord.

The objective of this work, then, was the development of an automatic mesh generation script for the mesh generation software *POINTWISE*®, that generated C-type meshes with parameters that a user could define from a global input file exterior to *POINTWISE*®, like suction patch length and position, and refinement. After that, the effects of suction on noise and aerodynamic performance for a given patch configuration and operating conditions were to be studied. Also, similar studies while varying suction patch configuration, namely length and position, were to be conducted, to ascertain which configuration benefited the most from suction, in terms of noise reduction and aerodynamic performance. Finally, another analogous study was conducted, this time varying the operating conditions, namely Mach number and Angle of Attack (AOA).

2. Implementation

The present section focuses on the steps needed to obtain to results, from the mesh generating scripts to the post correction of the computations.

2.1. Generating the Mesh

As previously mentioned, the first objective of the work was to create an automatic meshing script to work with a more recent software, to phase out the usage of the older IGG™. For the generation of the meshes used in the computations, *POINTWISE®*, a mesh generating software, was used. The goal of this first stage was to develop a script in Glyph2 – a scripting language developed for *POINTWISE®* that is an extension of the TCL language – capable of automatically generating a mesh for the CFD calculations, with a set of parameters the user could easily change through a global input file without any knowledge of the inner workings of *POINTWISE®*, while also fulfilling a set of requirements. The main requirements were: generate a C-Type mesh around an airfoil with a sharp trailing edge, given the coordinates file; refine the mesh on the location of the suction patches; attribute the correct boundary layer conditions; split the resulting mesh into 8 identically sized blocks to allow for faster, parallel computation; output a *.cgns* file compatible with the *cgns2flower* program. The script should also allow for the selection of the number of suction patches on the suction side of the airfoil; the beginning and end positions of each patch in fractions of the chord length – definition of patch position and length; the number of divisions in each patch; and the number of grid points in each patch.

With the help of Rouven Mayer's *POINTWISE®* script and Benjamin Arnold's IGG™ script, it was possible to understand the inner workings of the scripting process and produce a script that met all the requirements. Additionally, the code is nearly ready to automatically generate O-Type meshes, account for blunt trailing-edge airfoils and implement pressure side suction patches. Currently, it lacks a block splitting algorithm that predicts these situations and allows for proper splitting.

Figure 1 presents one of the used meshes, in this case with a suction patch on the suction side of the airfoil, starting at 57.5% of the chord and ending at 62.5%.

Further refinement was done around the suction patch itself, as made evident by Figures 2, which also displays the block splitting. This is representative of all the executed meshes. As for the resolution of the boundary layer, 60 layers were used, with a growth rate of 1.1, and a dimensionless wall distance of $y^+ = 0.125$, for good capturing of the boundary layer state, quintessential to understanding the effects of suction on it. In the presented case, each one of the eight blocks contains 10640 cells: 140 in the normal direction and 76 in the other, totalling 85120 cells for the entire mesh. Lastly, the farfield has the size of around 50 chord lengths in each direction.

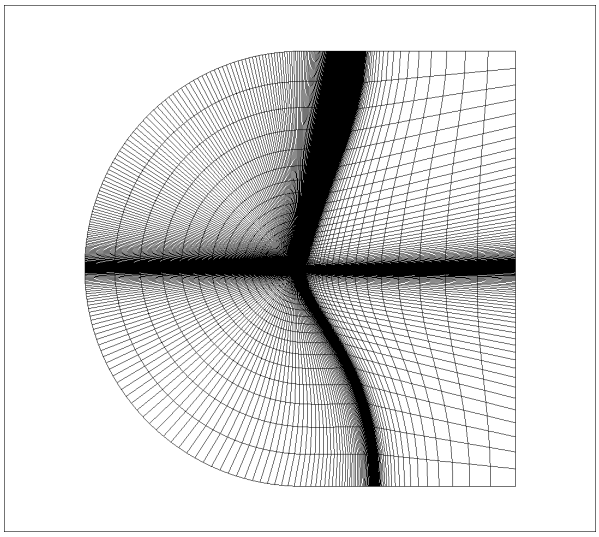

Figure 1: Full view of the generated C-type mesh for 0.575/0.625 suction patch case.

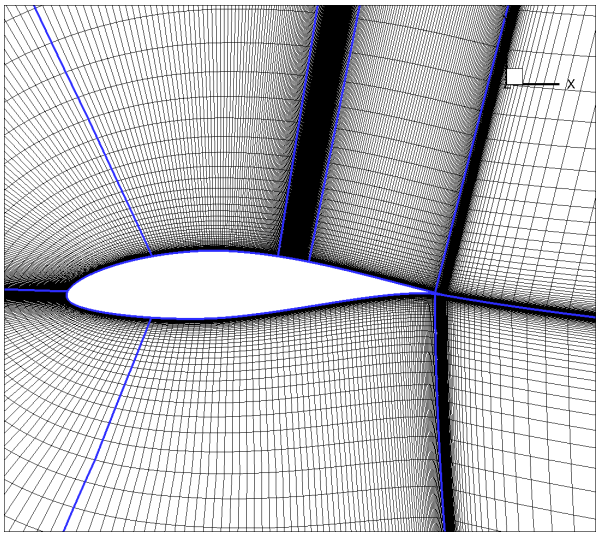

Figure 2: Detailed view of the generated C-type mesh for 0.575/0.625 suction patch case with block divisions in blue.

2.2. *cgns2flower*

cgns2flower is a program developed in IAG that serves as an interface between *POINTWISE®* and *FLOWer*. It takes the *.cgns* file generated by *POINTWISE®*, and outputs a set of files that will be used by *FLOWer* to perform the CFD computations.

2.3. Performing The Computations

For the computations themselves, *FLOWer* was used. *FLOWer* is a finite-volume, Structured Reynolds-Averaged Navier-Stokes (RANS) equations in integral form, in two or three dimensions, structured mesh solver developed by the Deutsches Zentrum für Luft- und Raumfahrt (DLR) – Institut für Aerodynamik und Strömungstechnik. It receives as input the files generated by *cgns2flower* and outputs the result files that allow the user to check the values of various flow parameters, convergence results, values of parameters at the surface of the airfoil, etc [26]. IAG developed a specific boundary condition for *FLOWer* to implement boundary layer blowing and suction, while also specifying whether the actuator works with constant pressure, constant suction velocity or a user defined suction profile along the suction regime. Also, in the data resulting from the *FLOWer* computations, there are the related turbulence input parameters for the subsequent noise prediction. The turbulence model used in the calculations was the Shear Stress Transport $k - \omega$ model.

It is worth mentioning that researchers at the IAG [27] have studied if the suction patch boundary condition used by *FLOWer* lacked accuracy, due to not considering friction and pressure loss effects of the porous plate, when compared to a more detailed CFD analysis with a properly 3D-modelled porous plate and suction chambers. They found out that going into such detail provided little difference between the results of both analysis when looking on the relevant boundary layer parameters and trailing edge noise results, thus concluding that the suction boundary condition used in *FLOWer* was perfectly usable for future research.

The airfoil chosen for the computations corresponds to a slice of a blade belonging to the wind turbine type that is being studied at the IAG. The slice was done at 83.34% of the total length of the blade (the slice is closer to the tip of the blade). This position was selected because it's closer to the tip of the blade, where most of the trailing edge noise comes from [5], but is still in the region where the flow can by considered 2-Dimensional, as previous studies done at the IAG pointed out. The resulting airfoil corresponds to a NACA 64_3-618 with a chord length of 2.5175 meters. The operating Reynolds and Mach numbers were 11049876 and 0.19, respectively. The AOA was 7.3°. The condition of suction applied in *FLOWer* is constant suction velocity. Also, transition has been forced at 5% of the chord both in the upper side and the lower side.

The first step of the computations consists in calculating results for each mesh and free-stream parameters without suction, for 210000 iterations. *FLOWer* then computes an additional 105000 iterations with suction enabled, in the cases were the suction mass flow is defined to be greater than 0. Finally, 52500 more iterations are computed, to get the mean of the results. Only then are the final results obtained.

2.4. *Rnoise*

Rnoise is an acoustic code developed by the IAG that makes use of an improvement to the TNO model to compute farfield noise spectra as well as theoretical wall pressure fluctuation spectra. It makes use of the resulting *FLOWer* data to achieve these results [13]. For the present work, *Rnoise* was used to verify the levels of sound reduction achieved via the employment of suction, as well as the changes this AFC mechanism effects on the frequency spectra of the different cases. It was an invaluable tool for this work.

2.5. Convergence Study

As is common procedure in CFD analyses, a convergence study was performed to evaluate the minimum number of mesh cells needed to achieve good results. To that effect, computations with increasing levels of mesh refinement were run, to determine the best relation of number of cells to computation time. These were all run for 210000 iterations each, for the baseline case with the suction patch starting at 57.5% of the chord and ending at 62.5%.

To determine convergence the results for the total coefficient of lift (c_l), total coefficient of pressure drag (c_{dp}), total coefficient of friction drag (c_d), and total coefficient of moment (c_m), were analyzed. The total number of cells, and the total time it took to conclude the computations was also registered, along with the residuals. In the end, a level of refinement that resulted in 85120 cells (10640 per block) was picked. The level of less refinement closest to it, with 71680 also presented good convergence results, sufficient for the current configuration. However, the bigger value was picked to ensure that convergence would not be compromised when using longer suction patches. The increased computation time was not seen as a too big of a hindrance, but rather a sensible compromise.

The residual was plotted, using a script developed by Benjamin Arnold, for the final values of the computations, meaning, after the 105000 iteration, suction enabled computations and the 52500 iteration, mean computations. A residual plots can be seen in Figure 3:

As can be observed, even a long patch has good levels of convergence, in the order of 10^{-8}. The peaks in the plots represent the beginning of new

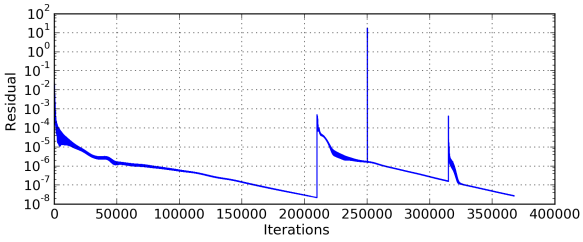

Figure 3: Final convergence results with 85120 cells for the 0.475/0.725 suction patch case, $cq = -0.004$.

calculations, hence their location at iteration number 210000 and 315000 (210000+105000). The reason for the other peak between these two is unknown.

2.6. Validating the Mesh

It was then necessary to validate the mesh. As Benjamin Arnold had validated results achieved with an IGG™ generated mesh, computations with the same airfoil, patch position, and flow parameters were done, so that the results could be compared. It was assumed that, if the results were very similar, it would be enough to validate the automatic meshing script. To that effect, the mean coefficient of pressure and friction results were plotted and compared, for the case with the suction patch starting at 57.5% of the chord and ending at 62.5%, with the value of coefficient of suction $cq = -0.002$ and $cq = -0.008$. The airfoil and free-stream parameters were the ones corresponding to the previously mentioned slice of the blade at 83.34% of its length. One of the comparisons can be seen in Figure 4:

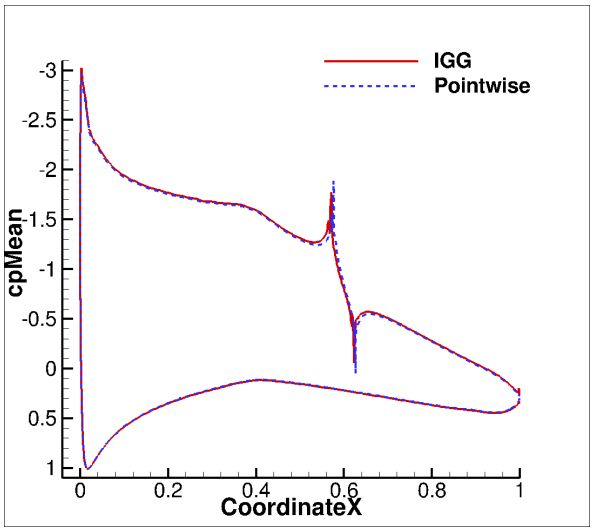

Figure 4: Comparison of mean coefficient of pressure results for the IGG and Pointwise generated meshes, with $cq = -0.008$.

Every comparison exhibited results with good agreement like the above. The main difference between the IGG™ and *POINTWISE*® results lies in the suction region, in which the *POINTWISE*® mesh allows for more precision in determining suction locations. It is thus considered the mesh to be validated. In regards to noise results (presented in the subsequent sections), those are also in general agreement with the achieved values of experimental noise reduction of around 6 dB with moderately high values of c_q ([-0.008;-0.016]) [27].

2.7. Post-Processing of the Results

After the final results of *FLOWer* were obtained, they had to be post-processed in two different aspects, so that they could be correctly visualized and be correctly interpreted by *Rnoise* on one hand, and on the other, have the correct c_l and c_d values. A minor post-processing operation consisted in organizing the results and computing the delta-values – for instance, the difference between the SPL of a suction enabled case and a baseline case – to be displayed properly in the well known CFD post-processing tool, *Tecplot*®.

The first important operation of post-correction involved taking the output files from *FLOWer* and changing the order of the points to comply with the *Rnoise* code and provide accurate visualization in *Tecplot*®. This is because *POINTWISE*® numbers the generated mesh blocks in a way that is not sequential, whereas the blocks, for accurate post-processing, should be numbered starting from the farfield pressure side block, around to the leading edge, and ending at the suction side farfield block. This, however, has no effect on the *FLOWer* computations. A solution in *POINTWISE*® itself to this problem is yet to be found. To solve it, a script in Python was written, to correctly find the blocks amidst the data and reorder them correctly.

The second important operation of post-correction involved making the necessary corrections to c_l and c_d values, due to suction. Volker Sailer, in his Master Thesis, warns that the momentum imparted to the flow due to suction has to be accounted for in the calculations, adding the resulting lift and drag corrections to the respective coefficients computed by *FLOWer* [28]. To that effect, he presents the formulas for the impulse components calculation:

$$I_{x'} = \int_{p_1}^{p_2} \rho v_{x'} \left(\vec{v'}\vec{n'}\right) ds, \tag{6}$$

$$I_{y'} = \int_{p_1}^{p_2} \rho v_{y'} \left(\vec{v'}\vec{n'}\right) ds, \tag{7}$$

where p_1 and p_2 are the beginning and end points of the patch, and s is the surface of the airfoil, $\vec{v'}$ is

the local surface velocity vector and $\vec{n'}$ is the normal vector to the surface of the airfoil, both rotated according to the AOA.

The impulse components then allow the calculations of the corrections to be applied to the coefficients, like so:

$$c_{dIx'} = \frac{2I_{x'}}{\rho_\infty v_\infty^2}, c_{lIy'} = \frac{2I_{y'}}{\rho_\infty v_\infty^2}, \quad (8)$$

where ρ_∞ and v_∞^2 are the air density and inflow velocity, respectively. Finally, these values are simply added to the *FLOWer* computed c_d and c_l respectively. For this process, another Python script was developed, having Benjamin Arnold's equivalent *MATLAB* script as an aid. Finally, as previously mentioned, a few extra Python scripts were written to compute the increase or decrease in SPL and the lift and drag coefficients of the suction enabled cases against their respective baselines, later organizing all these results in a format readable by *Tecplot*®, so that the plots in the subsequent chapters could be produced.

3. Results

In this section, the results pertaining to the analysis of a single suction patch, the analysis of varying patch configurations and varying free-stream parameters will be presented and explained.

3.1. Results for a Single Suction Patch

The first study made with the newly developed process chain aimed to discover the effects of suction on TEN and aerodynamic performance. The patch configuration under consideration is a single suction patch. Its start and end position, as well as operating conditions, were the same as the ones mentioned in the previous section. The c_q values analyzed were: 0.0 (baseline); -0.001; -0.002; -0.004; -0.008; -0.016.

3.1.1 Sound Pressure Level Results

This subsection begins with the analysis of the overall SPL reduction caused by suction. To that effect, Figure 5 shows the SPL for each value of c_q. In the absence of suction, the calculated SPL value was 76.6*dB*, whereas with the highest level of applied suction (c_q=-0.016), the noise was reduced to 71.4*dB*, a 5.2*dB* reduction, which is in line with the experimental values gathered by the IAG [23]. Despite the increase in the noise reduction with increasing suction, its rate actually decreases. In fact, the lowest level of suction (c_q=-0.001) is responsible for around 33% of the observed noise decrease, whereas with c_q=-0.002, more than 50% of the total noise decrease is achieved.

The reason for the abrupt decrease in noise as suction is applied can be detected when comparing the flow field plots of the baseline (no suction) and the c_q=-0.001 cases. Flow separation is occurs near the trailing edge of the airfoil in the baseline configuration, whereas absent in all the considered suction enabled cases. By eliminating separation, stalled flow noise can be avoided. Also, in Figure 6, the effects of suction on the boundary layer (BL) velocity and normalized turbulent kinetic energy (KTE) (k_T/U_∞^2) profiles can be seen, providing good insight on the reasons behind the noise reduction.

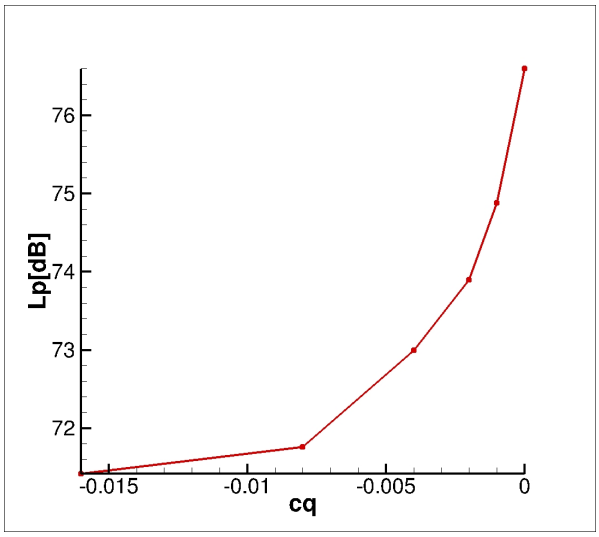

Figure 5: Decrease in SPL [dB] as a function of c_q.

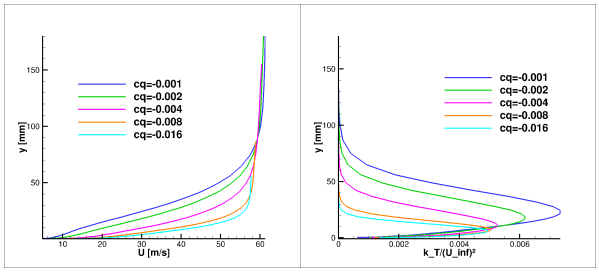

Figure 6: Boundary layer velocity (left) and normalised turbulent kinetic energy (right) profiles at the trailing edge for different c_q values. 0.575/0.625 case.

Due to separation, the baseline (no suction) result is not shown, as every value was calculated near the trailing edge, but it is easy to extrapolate it from the given data. As is made evident by Figure 6, suction has a definitive impact on the BL velocity and KTE profiles. The velocity of the BL near the wall is greatly increased by suction, whereas the thickness decreases substantially. As for KTE, its maximum is decreased and shifted towards the wall. The reduction in the BL thickness resulted

in smaller turbulent length scales, which, coupled with the reduction of the KTE, causes a reduction in the wall pressure fluctuations responsible for trailing edge noise [24].

In terms of the resulting noise frequency spectrum, the typical low frequency SPL peak due to TEN subsides, but the SPL level at higher frequency rises. This is a consequence of the increased KTE near the wall and the reduced turbulent length scales.

It can be observed that, when suction is disabled, the largest noise contribution comes from the suction side, at very low frequencies, as expected. When suction is applied, the SPL in the lower frequency region, on the suction side, is considerably reduced, bringing it to par with the pressure side results, and lowering the overall SPL. However, the SPL at higher frequencies is increased, which is a consequence of the increased KTE near the wall and the reduced turbulent length scales.

3.1.2 Aerodynamic Performance Results

The effects of suction in the aerodynamic performance of the blades are also important to consider, to determine if there are more potential benefits than noise reduction, or maybe even drawbacks. Hence, results pertaining the effects of c_q on c_l and c_d are the focus of this particular section, in the form of the c_l/c_d ratio, as shown by Figure 7:

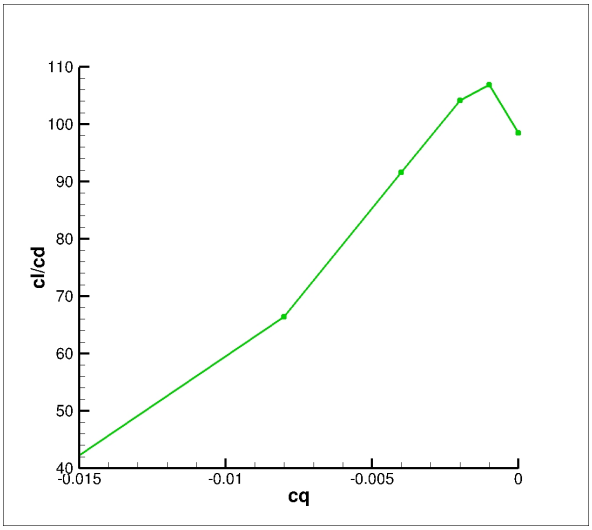

Figure 7: c_l/c_d as a function of c_q, for the baseline configuration.

This particular result is very important, as it shows that high levels of sound reduction imply a drawback in performance. While c_l is increased with suction, due to increased difference in the mean c_p between the suction side and the pressure side, at a diminishing rate, c_d is also increased when c_q¿-0.001, but at an increasing rate. The initial increase in performance is due to friction drag being reduced at a faster rate than the pressure drag increases, thus resulting in a decrease in overall c_d while c_l increases. This shows that high levels of c_q capable of significant noise reductions also significantly compromise performance. Thankfully, most of the noise reduction occurs at low levels of suction, as seen previously.

3.2. Results for Multiple Patch Configurations

In this subsection, the results for the studies conducted with multiple patch variations are presented. For these calculations, 7 different patch configurations were analyzed. Their characteristics, in fractions of chord length, are listed in Table 1:

Table 1: Dimension and Position of Suction Patch. Values correspond to chord fractions.

Beginning	End	Midpoint	Length
0.475	0.725	0.6	0.25
0.525	0.675	0.6	0.15
0.575	0.625	0.6	0.05
0.575	0.825	0.7	0.25
0.625	0.775	0.7	0.15
0.675	0.725	0.7	0.05
0.775	0.825	0.8	0.05

The values of the AOA, Reynolds number and Mach number were kept the same as the previous analysis.

3.2.1 Sound Pressure Level Results

First, the achieved SPL results are presented, in Figure 8.

In this figure, ΔL_p represents the difference in SPL between the baseline and the suction enabled cases. After analysing every result pertaining to the 0.775/0.825 case, it was deemed anomalous, despite a more downstream suction patches performing better in terms of sound reduction. In the above figure it can be seen that longer patches are more effective at reducing noise. It can also be seen that, the shorter the patch is, the more important is the position in their noise reducing capabilities. When analyzing the boundary layer parameters at the trailing edge, it could be seen that it is because the longer and more downstream patches are more effective at reducing boundary layer thickness and KTE.

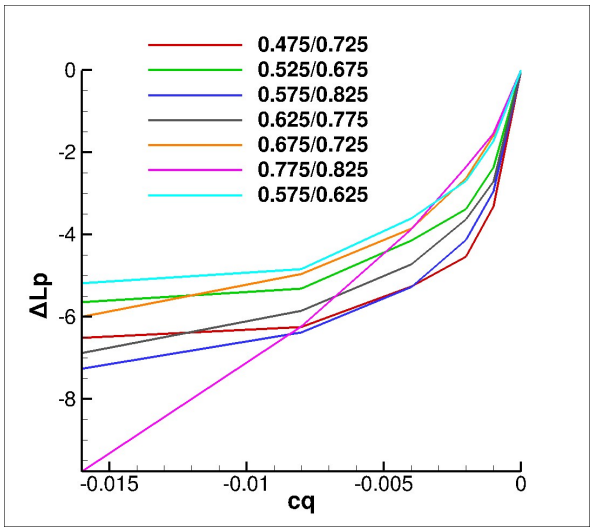

Figure 8: Results of the 7 different patch configurations – Decrease in SPL [dB] as a function of c_q.

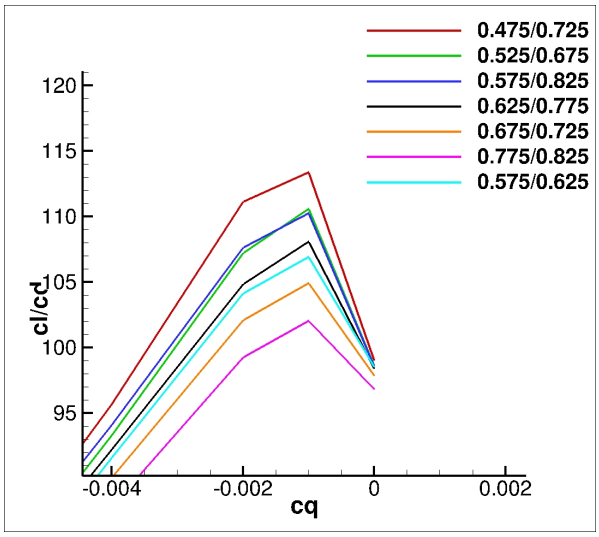

Figure 9: Detailed view of c_l/c_d as a function of c_q.

3.2.2 Aerodynamic Performance Results

As previously seen, suction has a dramatic effect on the aerodynamic performance of an airfoil. It is therefore very important to analyse which patch configuration benefits the most with low levels of suction, and is hampered the least by higher levels.

Figure 9 shows that the 0.475/0.725 is the patch that has its performance improved the most by suction. This is because the more upstream patches had a greater drag reduction with low suction levels compared to the downstream ones. This was due to the lower increase in c_l they experience with suction, and since c_l is related to the pressure drag coefficient, c_{dp}, this correlated to their drag results. The more downstream patches have a bigger difference between mean pressure coefficients of the suction and pressure sides of the airfoil, which explains their increased c_l when compared with upstream patches with the same suction level. Also, shorter patches show a bigger increase in c_l at higher levels of suction, due to the higher suction speed they require to meet achieve the target suction mass flow rate (smaller area requires greater flow velocity to maintain mass flow). This, in turn, increased the impulse contribution to the c_l. At the highest level of suction considered, all patch configurations had their c_l/c_d ratios reduced to around 40.

3.3. Free Stream Parameters Variation

Lastly, the results pertaining to an analogue analysis while varying the free-stream parameters, namely AOA and Mach number, was done.

3.3.1 Angle of Attack Variation

For this analysis, computations with AOA from 0° to 10°, in increments of 2° were done. The Reynolds and Mach numbers were again the same, at 11049876 and 0.19, respectively.

The plots of Figure 10 show that that higher AOA cases take a greater advantage of suction. This is because higher AOA implies a greater boundary layer thickness, KTE, and also flow separation. So the effects of suction are more dramatic on the higher AOA cases, since these factors are reduced at a higher rate. What is truly surprising is that the noise emitted by the higher AOA cases, when higher levels of suction are applied, is lower than the lower AOA cases, for the same suction level. This is due to the fact that the pressure side noise contribution decreases with increasing AOA, whilst the suction side contribution increases, thus increasing the potential for overall noise reduction. In regards to the aerodynamic performance, the results follow a more predictable pattern, as the higher AOA cases show the most benefit from suction. This is reasonable to be expected, since higher suction at higher AOA contributes dramatically to the c_l, since it reattaches the flow that was separated, even at low suction levels. Also, higher AOA cases also have much higher baseline drag levels, which suction dramatically reduces, thereby increasing the c_l/c_d ratio. This is important, as it allows the usage of increased suction values to compensate for the higher noise levels of high AOA airfoils with no suction enabled, therefore being more advantageous to use higher AOA in the blades. This, of course, doesn't take into account any energy consumption by suction actuators.

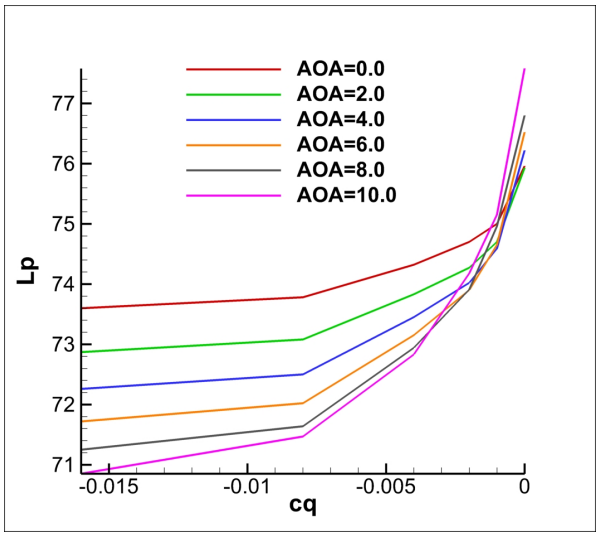

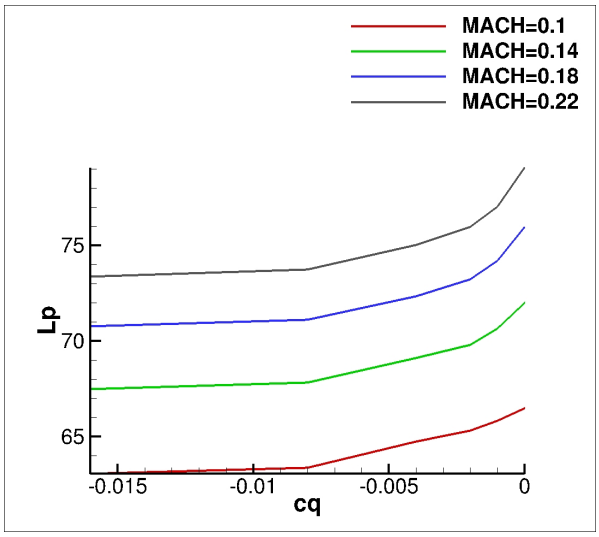

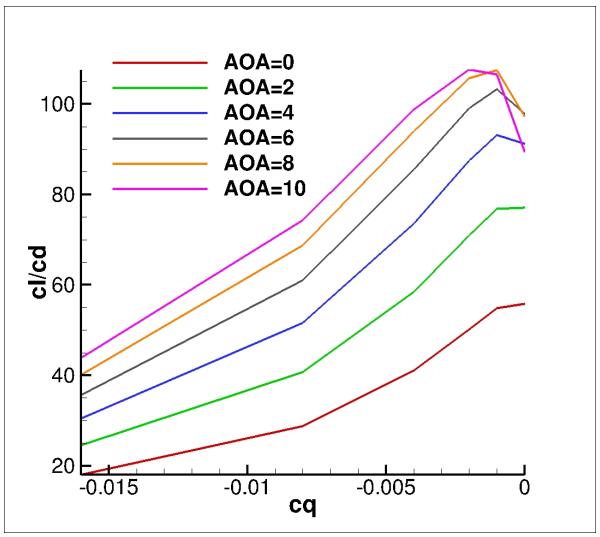

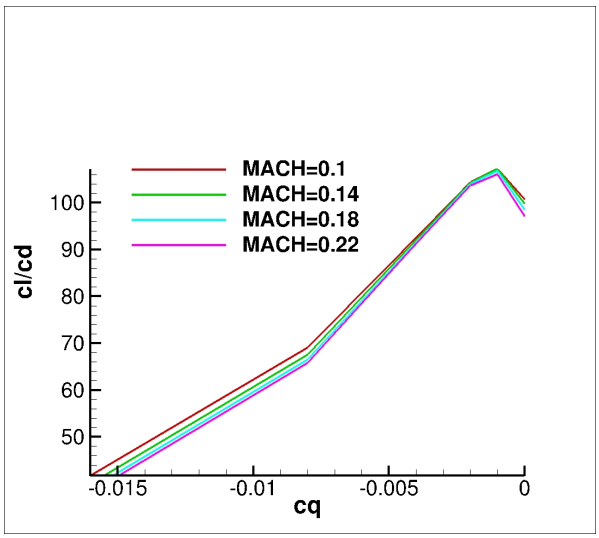

Figure 10: Top: Results of AOA variation – Absolute decrease in SPL [dB] as a function of c_q. Bottom: Variation of c_l/c_d as a function of c_q for different values of AOA.

Figure 11: Top: Results of Mach number variation – Absolute decrease in SPL [dB] as a function of c_q. Bottom: Variation of c_l/c_d as a function of c_q for different values of Mach number.

3.3.2 Mach Number Variation

Finally, for this analysis, computations with Mach number from 0.1 to 0.22 in increments of 0.04 were done. Reynolds number and AOA were kept at 11049876 and 7.3°, respectively.

Figure 11 shows the results obtained in this analysis. Higher Mach cases are the ones that benefit the most from suction, as their noise is reduced more than the lower cases. However, even with suction, higher Mach numbers still display higher noise levels. This is to be expected, since they have a "richer" BL velocity profile. As previously explained, this implies larger turbulent length scales, which in turn are responsible for the increase in noise. Of course, the KTE is also larger, with increasing Mach number. Having a richer BL velocity profile and more KTE means the effects of suction will be much more visible, and that's precisely what happens in this situation: the difference in the BL velocity profile and especially in the BL KTE profile when suction is applied is much larger for the higher Mach numbers as it is for the lower ones, thus explaining why the reductions are higher. In regards to the aerodynamic performance results, there is little to be said, as suction affects the performance in very similar fashion for all the cases.

4. Conclusions

The primary objective of this work, which was developing the automated mesh script, was completed, and it allowed for interesting analyses to be

done. From these, it was possible to see the effects of suction not only on noise reduction, but also aerodynamic performance. The results obtained were enlightening, as they showed that noise reduction via suction can implicate a large drop in performance. Therefore, more research should be done in order to find away to either delay the performance decrease from added suction, or increase the noise reduction at low levels of suction. The results also provided insight on the best patch configurations that can be picked, and also that suction has a greater impact on higher AOA operating conditions.

Future work should start by extending the mesh generation script to improve its versatility and available customization options. Conducting parallel research that focuses on the energy requirements for the suction actuators is also a good idea, as different patch configurations will have different energy requirements. Finally, before proceeding to more complex research on three-dimensional flow regimes, further investigation on the effects of suction with varying chord lengths should be conducted. Also, conducting a similar study for varying chord length is also a good extension to this topic.

Acknowledgements

I'd like to thank my supervisors, Professor Fernando Lau and Benjamin Arnold, for their assistance in the present work. I'd also like to thank the IAG for allowing me to perform this research and use the invaluable tools to achieve these results.

References

[1] Eja Pedersen and Högskolan I Halmstad. Noise annoyance from wind turbines: a review. Technical report, 2003.

[2] Karl Bolin, Gösta Bluhm, Gabriella Eriksson, and Mats E Nilsson. Infrasound and low frequency noise from wind turbines: exposure and health effects. *Environmental Research Letters*, 6(3):035103, 2011.

[3] Michael A Nissenbaum, Jeffery J Aramini, Christopher D Hanning, et al. Effects of industrial wind turbine noise on sleep and health. *Noise and Health*, 14(60):237, 2012.

[4] Stefan Oerlemans and Paul Migliore. Aeroacoustic wind tunnel tests of wind turbine airfoils. *AIAA paper*, 3042:2004, 2004.

[5] Stefan Oerlemans, P Sijtsma, and B Méndez López. Location and quantification of noise sources on a wind turbine. *Journal of sound and vibration*, 299(4):869–883, 2007.

[6] Siegfried Wagner, Rainer Bareiss, and Gianfranco Guidati. *Wind turbine noise*. Springer Science & Business Media, 1996.

[7] HMv Macdonald. A class of diffraction problems. *Proceedings of the London Mathematical Society*, 2(1):410–427, 1915.

[8] JE Ffowcs Williams and LH Hall. Aerodynamic sound generation by turbulent flow in the vicinity of a scattering half plane. *Journal of Fluid Mechanics*, 40(04):657–670, 1970.

[9] Taehyung Kim, Seungmin Lee, Hogeon Kim, and Soogab Lee. Design of low noise airfoil with high aerodynamic performance for use on small wind turbines. *Science in China Series E: Technological Sciences*, 53(1):75–79, 2010.

[10] S Oerlemans, JG Schepers, G Guidati, and S Wagner. Experimental demonstration of wind turbine noise reduction through optimized airfoil shape and trailing-edge serrations. Technical report, Nationaal Lucht-en Ruimtevaartlaboratorium, 2001.

[11] Stefan Oerlemans, Murray Fisher, Thierry Maeder, and Klaus Kögler. Reduction of wind turbine noise using optimized airfoils and trailing-edge serrations. *AIAA journal*, 47(6):1470–1481, 2009.

[12] René R Parchen and Technisch Physische Dienst TNO-TH. *Progress report DRAW: A prediction scheme for trailing edge noise based on detailed boundary layer characteristics*. TNO Institute of Applied Physics, 1998.

[13] Mohammad Kamruzzaman, Dimitrios Bekiropoulos, Alexander Wolf, Thorsten Lutz, and Ewald Krämer. Rnoise: A rans based airfoil trailing-edge noise prediction model. In *Proceedings20th AIAA/CEAS Aeroacoustics Conference (2014–3305)*, 2014.

[14] Thomas F Brooks, D Stuart Pope, and Michael A Marcolini. *Airfoil self-noise and prediction*, volume 1218. National Aeronautics and Space Administration, Office of Management, Scientific and Technical Information Division, 1989.

[15] MS Howe. Contributions to the theory of sound production by vortex-airfoil interaction, with application to vortices with finite axial velocity defect. In *Proceedings of the Royal Society of London A: Mathematical, Physical and Engineering Sciences*, volume 420, pages 157–182. The Royal Society, 1988.

[16] MS Howe. Noise produced by a sawtooth trailing edge. *The Journal of the Acoustical Society of America*, 90(1):482–487, 1991.

[17] Benshuai Lyu, Mahdi Azarpeyvand, and Samuel Sinayoko. A trailing-edge noise model for serrated edges. In *21st AIAA/CEAS Aeroacoustics Conference*, pages 1–24, 2015.

[18] A Tuck and Julio Soria. Active flow control over a naca 0015 airfoil using a znmf jet. In *15th Australasian fluid mechanics conference*, pages 13–17, 2004.

[19] M Goodarzi, M Rahimi, and R Fereidouni. Investigation of active flow control over naca0015 airfoil via blowing. *International Journal of Aerospace Sciences*, 1(4):57–63, 2012.

[20] Kianoosh Yousefi, S Reza Saleh, and Peyman Zahedi. Numerical investigation of suction and length of suction jet on aerodynamic characteristics of the naca 0012 airfoil. *International Journal of Materials, Mechanics and Manufacturing*, 1(2):136–142, 2013.

[21] MH Shojaefard, AR Noorpoor, A Avanesians, and M Ghaffarpour. Numerical investigation of flow control by suction and injection on a subsonic airfoil. 2005.

[22] Th. Lutz and A. Wolf. Active flow control for noise reduction and performance improvement of future generation wind turbines. 2009.

[23] W Würz, S Guidati, A Herrig, Th Lutz, and S Wagner. Measurement of trailing edge noise by a coherent particle velocimetry method. In *12th International conference on methods of aerophysical research ICMAR, Novosibirsk*, 2004.

[24] Thorsten Lutz, Benjamin Arnold, Alexander Wolf, and Ewald Krämer. Numerical studies on a rotor with distributed suction for noise reduction. In *Journal of Physics: Conference Series*, volume 524, page 012122. IOP Publishing, 2014.

[25] B. Arnold, Th. Lutz, E. Krämer, and D. Abzalilov. On the effect of boundary layer suction on the boundary layer state at the trailing-edge and noise reduction. February 2014.

[26] Deutsches Zentrum fr Luft-und Raumfahrt. *FLOWer Installation and User Manual*. 2008. Release 2008.1 mod.

[27] A. Wolf, Th. Lutz, and E. Krämer. Modelling of active flow control for noise reduction of future wind turbines. 2012.

[28] Volker Sailer. Untersuchung von Fluid Bumps zur Wellenwiderstandsreduktion mittels CFD. Master's thesis, Institut fr Aerodynamik und Gasdynamik der Universitt Stuttgart, Stuttgart, 2011.